Demonstration of double EIT using coupled harmonic oscillators and RLC circuits

Joshua Harden and Amitabh Joshi*
Department of Physics, Eastern Illinois University, Charleston, Illinois 61920

Juan D. Serna†
School of Mathematical and Natural Sciences, University of Arkansas at Monticello, Monticello, Arkansas 71656

(Dated: December 31, 2010)

Single and double electromagnetically induced transparency (EIT) in a medium, consisting of four-level atoms in the inverted-Y configuration, are discussed using mechanical and electrical analogies. A three coupled spring-mass system subject to damping and driven by an external force is used to represent the four-level atom mechanically. The equations of motion of this system are solved analytically, which revealed single and double EIT. On the other hand, three coupled RLC circuits are used, as the electrical analog, to explore and experimentally demonstrate single and double EIT. The simplicity of these two models makes this experiment appropriate for undergraduate students and easy to incorporate into a college physics laboratory.

PACS numbers: 01.50.My, 42.50.Gy, 42.50.Hz

I. INTRODUCTION

Atomic media have the physical characteristic of absorbing light of certain frequencies. It is possible, for example, that a medium absorbs two slightly different light frequencies simultaneously. However, and perhaps more intriguing, we observe that, for certain atomic configurations of the medium, the level of absorption of one of the frequencies can be controlled by the other frequency making the medium virtually transparent to the former frequency. This phenomenon is called electromagnetically induced transparency (EIT).[1] Usually, EIT occurs in vapors of three-level atomic systems, where laser lights (coherent light sources) drive two different atomic transitions sharing one common level (known as the "probe" and "coupling" field transitions). In the same way that a "coupling field" controls the properties of an EIT medium determining the amount of absorption of a "probe field", the dispersive properties of the medium also get modified resulting in to the reduction of the group velocity of light inside it. Physically, EIT can be understood as a process of quantum interference between two atomic states of a medium involving two indistinguishable quantum paths that lead to a common final state. In addition to the EIT phenomenon, double EIT occurs when a four-level atomic system is exposed to three laser sources driving three different transitions with one common level. The three transitions are described as the "probe", the "coupling", and the "pumping" field transitions. In this case, two strong electromagnetic fields, i.e., the coupling and the pumping fields control the medium in determining the absorption and propagation of the probe field.

The phenomenon of EIT, first observed two decades ago using high-power lasers in strontium vapor,[2] has been extensively investigated during the past years in atomic beams,[3] plasma,[4] optical cavities,[5] and Bose-Einstein condensates.[6] It has also been studied theoretically and experimentally for media consisting of three- and four-level atoms.[7,8]

Besides absorption of light, there are other substantial changes observed if a medium exhibits EIT, such as the modified index of refraction,[9] which can give rise to the reduction of the group velocity of a light pulse,[10] or even a complete stop of light in the medium.[11] Important applications of EIT include lasing without population inversion,[12] enhanced nonlinear optical processes,[13] quantum computation and telecommunications,[14] quantum memory,[15] and optical switches.[16]

During the past two decades, the study of quantum-classical analogies in physics has gained some momentum as they prove to be very useful in helping to understand the fundamental physical concepts and the applicability of different theories.[17] It is important to note that these analogies bring to light the fact that similar mathematical models can be applied to both quantum and classical phenomena, though these theories differ both in formalism, and fundamental concepts. Recently, a number of these classical analogies of different quantum optical systems have been reported. For example, stimulated resonance Raman effect,[18] rapid adiabatic passage in atomic physics,[19] vacuum Rabi oscillation,[20] number-phase Wigner function and its relation to usual Wigner function,[21] and EIT in three-level systems.[22] In a recent work, the response of a coupled array of nonlinear oscillators to parametric excitation is calculated in the weak nonlinear limit using secular perturbation theory and the exact results for small arrays of oscillators are used to guide the analysis of the numerical integration of the model equations of motion for large arrays. Such results provide qualitative explanations for experiments involving a parametrically excited micromechanical resonator array.[23]

Double EIT phenomenon is very important in EIT based atomic memory systems. Systems displaying multiple EIT could be useful in the bifurcation of quantum information in multiple channels temporarily, which then can be used in multiplexing required in certain quantum information protocols. The release of stored information

from multiple channels could be separately controlled by manipulating the group velocity of individual channels (via their control fields) in such systems. Hence double EIT is an important phenomenon for quantum information processing and quantum computing and thus, it needs its introduction and realization in the simplest form to the readers.

The goal of this work is to demonstrate double EIT in four-level systems using two classical analogies: mass-spring systems and RLC circuits. For that purpose, we first describe the atom as a damped, harmonic oscillator driven by an external force.[24] Three different masses connected by springs and subject to frictional forces (damping) are used to represent the four-level atom. The destructive interference of the normal modes of oscillation of the masses is equivalent to the quantum interference that originates EIT. Secondly, we explore experimentally, the electrical analogue of double EIT using three coupled RLC circuits. The power delivered to one of these coupled oscillating circuits is measured as a function of the frequency of a driving source of alternating voltage. The electrical equivalence of the power transmitted to the circuit with the power absorbed by an atomic medium, allows us to investigate, directly from the circuit, the characteristic patterns of single and double EIT.

To get information about the absorption and dispersion of light in the four-level atomic medium, we need to solve a large system of the density matrix equations numerically.[8] However, the equations of motion that describe the mechanical and electrical systems can be solved analytically and hence the double EIT phenomenon could be studied with more ease in the two analogue systems using the analytical solutions. The merit of analytic solutions is that it clearly brings out the functional dependence of double EIT phenomenon on several parameters. On the other hand, the circuits used in this experiment show realistic forced, damped harmonic oscillations that can be easily built and may be incorporated into an undergraduate physics laboratory, and help students and teachers to appreciate the complex quantum phenomena of EIT and double EIT put together in a very simplified manner both theoretically and experimentally.

II. MODEL AND BASIC EQUATIONS

We considered a medium consisting of four-level atoms in the so-called inverted-Y configuration as shown in FIG. 1. The levels $|1\rangle$ and $|2\rangle$ were coupled by a "probe" field of frequency ω, in whose absorption and dispersion we were interested. The level $|2\rangle$ was connected to the lower level $|0\rangle$ by a strong "coupling" field of frequency ω_c, and to the upper level $|3\rangle$ by the strong "pumping" field of frequency ω_r. Only the atomic transitions $|1\rangle \leftrightarrow |2\rangle$, $|0\rangle \leftrightarrow |2\rangle$, and $|2\rangle \leftrightarrow |3\rangle$ were dipole allowed.

In a typical double EIT experiment, quantum interference is introduced by driving the upper two levels with strong coherent fields. Under appropriate conditions, the

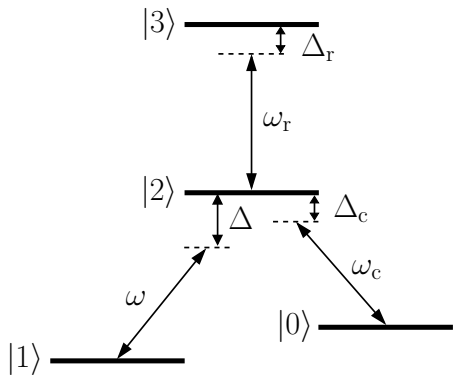

FIG. 1. Schematic energy level diagram of a four-level system in the inverted-Y configuration. Here ω, ω_c, and ω_r are the frequencies of the probe, coupling and pumping fields, respectively; whereas Δ, Δ_c, and Δ_r are their corresponding frequency detunings.

medium becomes *transparent* (zero absorption) for the probe field. In the absence of the coupling and pumping fields, we may observe a regular absorption resonance profile. However, under certain conditions, the addition of either the coupling or pumping fields prevents the absorption of energy by the medium, and the transmitted intensity as a function of the probe frequency shows a narrow peak of induced transparency called single EIT (or just EIT). When both coupling and pumping fields are simultaneously present, then they together control the absorption and propagation of the probe field, and thus double EIT may be observed in the transmitted intensity profile of the probe field.[25]

Absorptive and dispersive properties of the atomic system can be studied by calculating the electrical susceptibility of the system. When the atom-field interaction is determined by the density matrix equation and the corresponding off-diagonal (coherence) component of the probe transition is ρ_{12}, the complex susceptibility χ is given by $\chi = \mu_p \rho_{12}/E_p$, in which μ_p and E_p represent the dipole moment and the field amplitude for the probe transition. The susceptibility $\chi = \chi' + i\chi''$ is a complex quantity such that its real (imaginary) part determines the dispersive (absorptive) property of the atomic medium for the probe field. The intensities of the driving fields determine the effects observed in double EIT, as depicted in FIG. 2 for the radiative decay constants $\gamma_1 = \gamma_2 = \gamma_3 = 1.0$, and $\gamma_0 = 10^{-4}$. The Rabi frequencies Ω_c and Ω_r are directly proportional to the coupling and pumping field strengths, respectively, and must be comparable with all damping rates γ_i present in the medium.

Figure 2(a) clearly shows double EIT (two dips at $\Delta = 0$) at the exact resonance conditions of the coupling and pumping fields, i.e., $\Delta_c = \Delta_r = 0$ and ($\Omega_c = 1.0$, $\Omega_r = 2.5$). The corresponding dispersive property is given in FIG. 2(b). Furthermore, strong coupling and pumping fields may induce AC-Stark splitting of the ex-

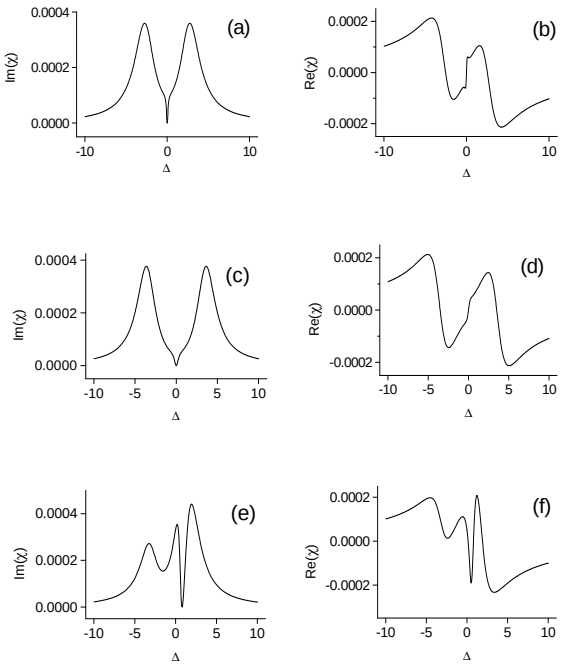

FIG. 2. Imaginary and real parts of the susceptibility χ, as a function of probe detuning Δ, for different parametric conditions. The profiles show double EIT for a four-level atom in an inverted-Y configuration with $\gamma_1 = \gamma_2 = \gamma_3 = 1.0$, and $\gamma_0 = 10^{-4}$. The other parameters for plots (a,b), (c,d), and (e,f) are ($\Omega_c = 1.0$, $\Omega_r = 2.5$, $\Delta_c = 0$, $\Delta_r = 0$), ($\Omega_c = 2.0$, $\Omega_r = 3.0$, $\Delta_c = 0$, $\Delta_r = 0$), and ($\Omega_c = 1.0$, $\Omega_r = 2.0$, $\Delta_c = 0.8$, $\Delta_r = 1.8$), respectively. All the parameters have the dimension of frequency.

cited levels $|2\rangle$ and $|3\rangle$ under resonant conditions. When the coupling and pumping fields are strong, the splitting expands, and the absorption spectrum displays the Autler-Townes doublets.[26] In FIG. 2(c), the values of the coupling and pumping fields Rabi frequencies are stronger ($\Omega_c = 2.0$, $\Omega_r = 3.0$ with other parameters unchanged) in comparison to FIG. 2(a) and hence the width of the two EIT dips becomes broader due to a wider splitting of the Autler-Townes doublets. The corresponding dispersive properties under this parametric condition are displayed in FIG. 2(d). Finally, the effect of off-resonant coupling and pumping fields ($\Omega_c = 1.0$, $\Omega_r = 2.0$, $\Delta_c = 0.8$, $\Delta_r = 1.8$) are displayed in FIG. 2(e,f).

Two EIT dips moved away from the $\Delta = 0$ position because of finite detunings of the coupling and pumping fields. The details of this theoretical work on double EIT are discussed in reference.[8] The single EIT observed experimentally in a three-level Λ-type atomic system, and double EIT in a four-level tripod type atomic system are shown in figure 4 of Ref. 27 and figure 3(a1) of Ref. 28, respectively. Clearly in the optical spectrum, a single deep is observed in the absorption spectrum of a single EIT system and two deeps are observed in a double EIT system. The experimental conditions are mentioned in the captions of the figures and can be further explored in those references.

A. Mechanical spring analog of single and double EIT-like phenomena

The Lorentz model[24,29] is recognized as one of the classical models for the atom that works incredibly well for describing the interaction of light with matter. The basic assumption made in this model is that the bounded electrons within the neutral atom oscillate about their equilibrium position with a very small amplitude. In addition, each electron-ion pair behaves as a simple harmonic oscillator which couples to the electromagnetic field through its electric dipole moment. Thus, the atom can be described as a damped harmonic oscillator of mass m attached to a rigid support by a spring of force constant κ and driven by a harmonic force $F = F_0 e^{-i(\omega t+\phi)}$. The inclusion of a damping force is necessary in the model because different physical processes, like atomic collisions and radiative decays, may take away energy from the atom. The forces acting on the oscillator (with its natural frequency $\omega_0 = \sqrt{\kappa/m}$) are the harmonic driving force F, the spring force $-\kappa x$, and the damping force $2\beta\dot{x}$, where $\dot{x}$ is the oscillator's speed. Newton's second law gives the equation of motion for the position variable x in the Lorentz model as

$$\ddot{x} + 2\beta\dot{x} + \omega_0^2 x = F_0 e^{-i(\omega t+\phi)}\,. \tag{1}$$

In the classical model of double EIT, we described the atom as a damped harmonic oscillator of mass m_1 attached to a rigid support by a spring of force constant κ_1 and driven by a harmonic force $F = F_0\, e^{-i(\omega t+\phi)}$. To this mass-spring combination were attached two other masses originally at rest, m_2 and m_3 that were connected to mass m_1 by springs of force constants κ_{12} and κ_{13}, respectively. These two masses were also fixed, from the other side, to rigid supports by springs of force constants κ_2 and κ_3, respectively [see FIG. 3(a)].

It is always a matter of importance and interest to know at what rate energy is transmitted into the driven oscillator, and how this power is absorbed as a function of the frequency ω.[30] In the typical situation of a damped harmonic oscillator m_1 driven by a harmonic force F, a standard absorption resonance profile is observed. However, if either m_2 or m_3 is allowed to move due only to the forces from the springs they are attached to (with force constants κ_{12} and κ_2, and κ_{13} and κ_3, respectively), this will avoid absorption in a limited region of the resonance profile, and the transmitted power as a function of the driving force frequency will show a narrow peak of induced transparency (single EIT).[22]

In this physical model of the atom, the spring attaching masses m_1 and m_2 (with force constant κ_{12}) emulated the coupling field between atomic levels $|0\rangle$ and $|2\rangle$, whereas the spring connecting masses m_1 and m_3 (with force constant κ_{13}) emulated the pumping field between

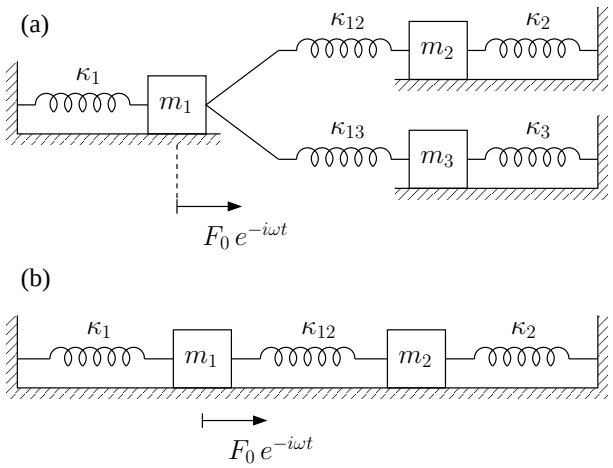

FIG. 3. Coupled damped harmonic-oscillator model showing (a) double EIT and (b) single EIT features.

levels $|2\rangle$ and $|3\rangle$. The probe field was then modeled by the harmonic force acting on mass m_1. These analogues remind us the description of the fields in terms of harmonic oscillators.[31] Now, if we allow *both* masses m_2 and m_3 to move simultaneously under the conditions described above, we will observe double EIT features.

To describe the classical evolution of this system, we used a fixed set of one-dimensional Cartesian coordinates x_1, x_2, and x_3, representing the positions of the masses from their equilibrium positions. Thus, the equations of motion could be written like

$$\begin{aligned} &\ddot{x}_1(t) + \gamma_1\,\dot{x}_1(t) + \omega_1^2\,x_1(t) \\ &\quad - \Omega_{\rm c}^2\,x_2(t) - \Omega_{\rm r}^2\,x_3(t) = (F_0/m)\,e^{-i\omega t}, \\ &\ddot{x}_2(t) + \gamma_2\,\dot{x}_2(t) + \omega_2^2\,x_2(t) - \Omega_{\rm c}^2\,x_1(t) = 0, \\ &\ddot{x}_3(t) + \gamma_3\,\dot{x}_3(t) + \omega_3^2\,x_3(t) - \Omega_{\rm r}^2\,x_1(t) = 0, \end{aligned} \tag{2}$$

where we assumed that $\phi = 0$ and $m_1 = m_2 = m_3 \equiv m$. The other parameters were defined as follows: $\omega_1^2 = (\kappa_1+\kappa_{12}+\kappa_{13})/m$, $\omega_2^2 = (\kappa_2+\kappa_{12})/m$, $\omega_3^2 = (\kappa_3+\kappa_{13})/m$, $\Omega_{\rm c}^2 = \kappa_{12}/m$, and $\Omega_{\rm r}^2 = \kappa_{13}/m$. The damping parameters γ_i (viscous damping) represented the mechanical equivalent to the spontaneous decay rates of the three excited states in the inverted-Y atomic configuration.

Because we expected the motion to be oscillatory, we attempted solutions of the form $x_i = B_i\,e^{-i\omega t}$, with B_is are constants ($i = 1, 2, 3$). Substituting these expressions for the displacements into the equations of motion, we found that the displacement of m_1 (atom displacement) was given by

$$x_1(t) = \frac{(F_0/m)\,e^{-i\omega t}}{(\omega_1^2 - \omega^2 - i\,\gamma_1\,\omega) - \dfrac{\Omega_{\rm c}^4}{\omega_2^2 - \omega^2 - i\,\gamma_2\,\omega} - \dfrac{\Omega_{\rm r}^4}{\omega_3^2 - \omega^2 - i\,\gamma_3\,\omega}}\,. \tag{3}$$

In the Lorentz oscillator model,[24,29] the electrical polarization $\mathcal{P}$ (or the susceptibility $\chi = \mathcal{P}/F$) induced in the atom by the external force field F is directly proportional to x_1, for the polarization is defined as $\mathcal{P} = N\,e\,x_1$, where N is the number of atoms per unit volume, and e is the electronic charge. The real and imaginary parts of x_1 give the dispersion and absorption properties of the atom, respectively. A graphical analysis of (3) will allow us to explore these two important properties of light propagation. The frequency differences (detuning) of the probe, coupling, and pumping fields with respect to the external driving field were defined like $\Delta = \omega_1 - \omega$, $\Delta_{\rm c} = \omega_2 - \omega$, and $\Delta_{\rm r} = \omega_3 - \omega$, respectively. These definitions are slightly different from what is used in optical double EIT nomenclature.[8]

B. Electrical analog of double EIT: coupled RLC circuits

There is a well known correspondence between a driven damped harmonic oscillator and an electrical circuit consisting of a resistor R, an inductor L, and a capacitor C connected in series to an alternating voltage source V.[32] The importance of this correspondence is that RLC circuits are easy to build in the laboratory, and may be used as excellent examples of *non mechanical* oscillations. We used these circuits to demonstrate experimentally and study theoretically single and double EIT by analyzing the dissipation of electric power in the resistance. The circuit that showed double EIT behavior is shown in FIG. 4(a). This circuit was made up of three loops of RLC circuits. The resistance, inductance, and capacitance of the loops were represented by R_i, L_i, and C_i, respectively ($i = 1, 2, 3$). The first loop with resistance R_1, inductance L_1, capacitances C_1 and $C/2$, represented the atom. The resistance accounted for the spontaneous radiative decay of the second excited level $|2\rangle$ to level $|1\rangle$. The capacitance C, shared by the first and second loops, provided the link between the atom and the coupling field; whereas the other capacitance C, shared by the first and third loops, linked the atom with the pumping field.

In this circuit, the loop that modeled the atom (loop 1) had a resonance frequency that represented the transition energy from the ground state $|1\rangle$ to the excited state

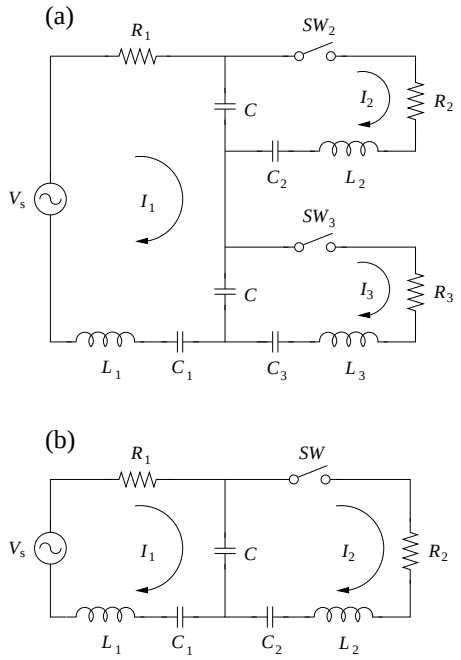

FIG. 4. Coupled RLC electrical circuits displaying (a) double EIT-like and (b) single EIT-like features.

$|2\rangle$. The probability of populating this excited state was a maximum when the alternating voltage source V was in resonance with the resonance frequency of this loop, (or in resonance with the $|1\rangle \rightarrow |2\rangle$ transition). However, with a three-loop configuration, we had two other possible ways to accomplish this excitation since we were using the analogue of a four-level atom in the inverted-Y configuration. For instance, loop 1 (representing the atom) could also have been excited either by the *coupling* loop 2 ($|0\rangle \rightarrow |2\rangle$), the *pumping* loop 3 ($|3\rangle \rightarrow |2\rangle$), or both.

The EIT was studied by examining the frequency dependence of the transmitted power from the voltage source $V = V_{\rm s}\, e^{-i\omega t}$ to the resonant first loop. If the currents flowing in the three different loops of the circuit are written like $I_1(t) = \dot{q}_1(t)$, $I_2(t) = \dot{q}_2(t)$, and $I_3(t) = \dot{q}_3(t)$, the following system of coupled differential equations for the charges is found

$$\begin{aligned} &\ddot{q}_1(t) + \gamma_1\, \dot{q}_1(t) + \omega_1^2\, q_1(t) \\ &\quad - \Omega_{\rm c}^2\, q_2(t) - \Omega_{\rm r}^2\, q_3(t) = (V_{\rm s}/L_1)\, e^{-i\omega t}, \\ &\ddot{q}_2(t) + \gamma_2\, \dot{q}_2(t) + \omega_2^2\, q_2(t) - \Omega_{\rm c}^2\, q_1(t) = 0, \\ &\ddot{q}_3(t) + \gamma_3\, \dot{q}_3(t) + \omega_3^2\, q_3(t) - \Omega_{\rm r}^2\, q_1(t) = 0, \end{aligned} \tag{4}$$

where $\gamma_i = R_i/L_i$, $\omega_i^2 = 1/(L_i C_{ei})$ (with $i = 1, 2, 3$), and $\Omega_{\rm c}^2 = \Omega_{\rm r}^2 = 1/(L_1 C)$. The equivalent capacitances for these loops were

$$\begin{aligned} C_{\rm e1} &= \frac{(C/2)\, C_1}{C/2 + C_1}, \\ C_{\rm e2} &= \frac{C\, C_2}{C + C_2}, \\ C_{\rm e3} &= \frac{C\, C_3}{C + C_3}. \end{aligned} \tag{5}$$

It was easy to compare (2) with (4) and conclude that both models described the same physical phenomenon.

Applying the Kirchhoff's second law to the three loops of the circuit,[33] with loop currents I_1, I_2, and I_3, we obtained

$$\begin{aligned} &[R_1 - i(2X_C + X_{C_1} - X_{L_1})]I_1 \\ &\qquad + iX_C I_2 + iX_C I_3 = V, \\ &iX_C I_1 + [R_2 - i(X_C + X_{C_2} - X_{L_2})]I_2 = 0, \\ &iX_C I_1 + [R_3 - i(X_C + X_{C_3} - X_{L_3})]I_3 = 0, \end{aligned} \tag{6}$$

where $X_C = 1/(\omega\, C)$ and $X_{C_i} = 1/(\omega\, C_i)$ ($i = 1, 2, 3$) were the capacitive reactances, and $X_{L_i} = \omega L_i$ ($i = 1, 2, 3$) were the inductive reactances. From the above system of equations, it was found that

$$I_1 = \left(\frac{A + iB}{A^2 + B^2}\right) V, \tag{7}$$

where, for convenience, we defined

$$A \equiv R_1 + \frac{R_2 X_C^2}{R_2^2 + [X_{L_2} - (X_C + X_{C_2})]^2} + \frac{R_3 X_C^2}{R_3^2 + [X_{L_3} - (X_C + X_{C_3})]^2}, \tag{8}$$

$$B \equiv X_{L_1} - (2X_C + X_{C_1}) - \frac{X_C^2[X_{L_2} - (X_C + X_{C_2})]}{R_2^2 + [X_{L_2} - (X_C + X_{C_2})]^2} - \frac{X_C^2[X_{L_3} - (X_C + X_{C_3})]}{R_3^2 + [X_{L_3} - (X_C + X_{C_3})]^2}. \tag{9}$$

The electrical power in the $R_1 L_1 C_{\rm e1}$ loop was obtained by multiplying (7) by the voltage. In-phase and out-of-phase components of the power were associated with the energy dissipated by the resistive ($P_{\rm R}$), and the energy stored by the reactance ($P_{\rm X}$) parts of the circuit, giving the following expressions

$$P_{\rm R} = \frac{A\,|V_{\rm s}|^2}{A^2 + B^2} \qquad \text{and} \qquad P_{\rm X} = \frac{B\,|V_{\rm s}|^2}{A^2 + B^2}, \tag{10}$$

where A and B were given by (8) and (9).

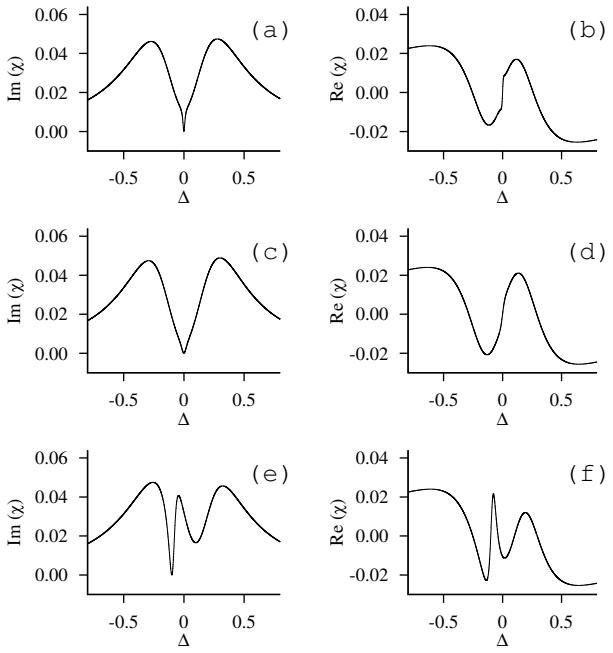

FIG. 5. Imaginary and real parts of the susceptibility χ for the double EIT-like system as a function of the detuning Δ. The radiative decays are $\gamma_1 = 1.0$, $\gamma_2 = 0.1$, $\gamma_3 = 10^{-4}$, and the coupling and pumping detunings $\Delta_c = \Delta_r = 0$. For plots (a) and (b): $\Omega_c = 3.0$, and $\Omega_r = 2.3$. For plots (c) and (d): $\Omega_c = 2.7$ and $\Omega_r = 3.0$. Plots (e) and (f) have $\Delta_c = \Delta_r = 0.1$ and $\Omega_c = 3.0$ and $\Omega_r = 2.3$. All the parameters have the dimension of frequency.

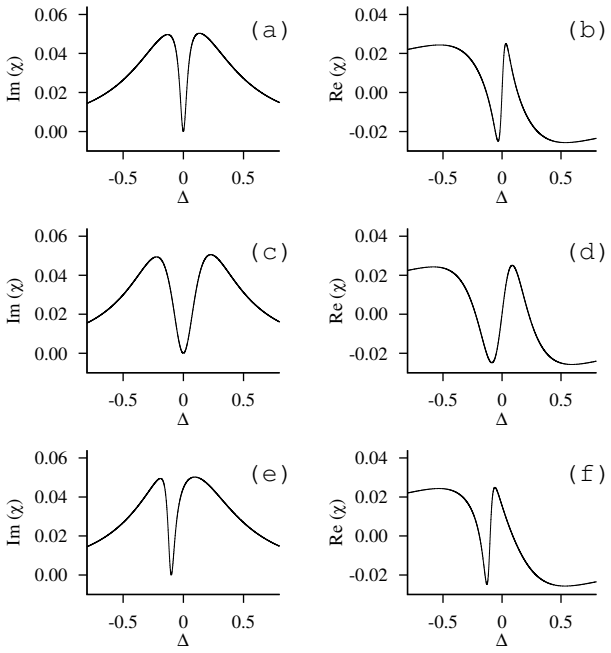

FIG. 6. Imaginary and real parts of the susceptibility χ for the single EIT-like system as a function of the detuning Δ. The radiative decays are $\gamma_1 = 1.0$, $\gamma_2 = 10^{-4}$, and $\gamma_3 = 0.0$. For plots (a) and (b), $\Delta_c = 0.0$ and $\Omega_c = 2.3$. For plots (c) and (d), $\Delta_c = 0.0$ and $\Omega_c = 3.0$. Plots (e) and (f), $\Delta_c = 0.1$ and $\Omega_c = 2.3$. All the parameters have the dimension of frequency.

We first studied the absorption and dispersion properties of the spring-mass system at exact resonance conditions $\Delta_c = \Delta_r = 0$ of the coupling and pumping fields. Figures 5(a) and 5(b) display the curves for the absorption and dispersion of the probe field, respectively. The Rabi frequencies and radiative decays (damping) used were $\Omega_c = 3.0$, $\Omega_r = 2.3$, $\gamma_1 = 1.0$, $\gamma_2 = 0.1$, and $\gamma_3 = 10^{-4}$ (all these quantities given in units of the atomic decay γ_1). Double EIT was observed in the absorption curve at $\Delta = 0$, where two dips of different widths, one inside the other, clearly became visible [FIG. 5(a)]. When the coupling and pumping frequencies were changed to $\Omega_c = 2.7$ and $\Omega_r = 3.0$, we noticed from the absorption curve that when the pumping field increased reducing its relative difference with the coupling field, the second dip became wider [FIG. 5(c)]. On the other hand, FIG. 5(d) shows how, in the vicinity of $\Delta = 0$, the peaks of dispersion flipped in a smoother way. The change of frequency detunings brought in further interesting changes as depicted in FIG. 5(e) and 5(f), where we set $\Delta_c = \Delta_r = 0.1$. Because of these detuning changes, the two EIT peaks separated from each other, and moved away relative to the $\Delta = 0$ position.

The double EIT features changed to those of single EIT [for the spring-mass system in FIG. 3(b)] when the zero-limit condition for either the coupling or pumping fields were considered (i.e., $\Omega_c = 0$ or $\Omega_r = 0$). The absorption and dispersion curves showed characteristics of standard EIT, as observed in FIG. 6(a) and 6(b), respectively. The parameters used for this case were $\Omega_c = 2.3$, $\Omega_r = 0.0$, $\gamma_1 = 1.0$, $\gamma_2 = 10^{-4}$, and $\gamma_3 = 0.0$. The effects of the coupling field strength on this system are now shown in FIG. 6(c) and 6(d). The only parameter changed was $\Omega_c = 3.0$. The broadening in the EIT peak was apparent and caused by the coupling field increase. In FIG. 6(e) and 6(f), the only parameter changed was $\Delta_c = 0.1$, leaving the other parameters as before. Clearly, the EIT moved away from the centre of the graph.

We next looked at the behavior of P_R and P_X as a function of the frequency detuning $\delta = \omega - \omega_R$ for different initial conditions of the parameters R, L, and C. In FIG. 7, the effects of the coupling and pumping frequency detunings, in the double EIT scenario, are shown when parameters L_2 and L_3 took on different values. The solid and dashed lines represent the absorption and dispersion of light, respectively. Figure 7(a) shows that, at exact resonance conditions for both the coupling and pumping fields with the probe field ($\Delta_c = \Delta_r = 0$), there was only a single dip in the curve (like single EIT). This happened because both EIT dips occurred at the same location. The corresponding dispersion curve also shows this particular characteristic. A separation of the two

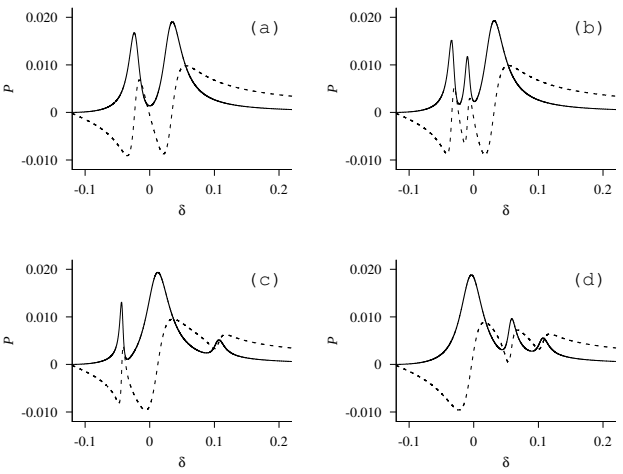

FIG. 7. Power transferred to the $R_1L_1C_{e1}$ circuit (Fig.6(a)) as a function of the detuning $\delta \equiv \omega - \omega_R$. This detuning was defined as the difference between the driving field frequency ω and the resonance frequency of the circuit ω_R. The parameters used were $R_2 = R_3 = 5.0\,\Omega$, $R_1 = 50\,\Omega$, $C_1 = C_2 = C_3 = 0.1\,\mu$F, $C = 0.2\,\mu$F, and $L_1 = 0.0010$ H. For plots (a) $L_2 = 0.0010$ H and $L_3 = 0.0010$ H; (b) $L_2 = 0.0010$ H and $L_3 = 0.0015$ H; (c) $L_2 = 0.0020$ H and $L_3 = 0.0003$ H; and (d) $L_2 = 0.0005$ H and $L_3 = 0.0003$ H. The solid line represents P_R, whereas the dashed line represents P_X. P is given in arbitrary units.

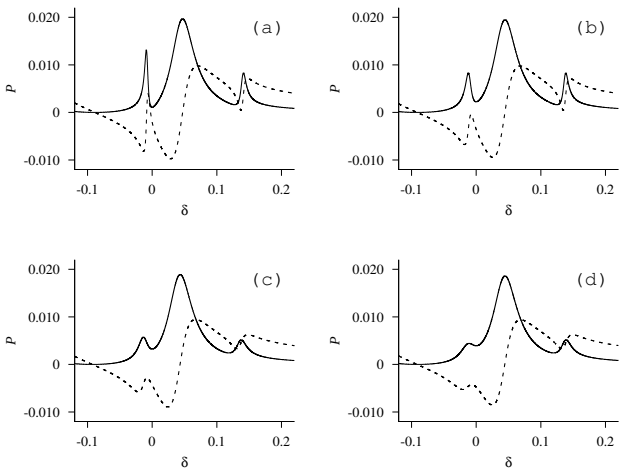

FIG. 8. Power transferred to the $R_1L_1C_{e1}$ circuit (Fig.4(a)) as a function of the detuning δ. The parameters used were $R_1 = 50\,\Omega$, $L_2 = 0.0020$ H, $L_1 = 0.0010$ H, $L_3 = 0.0003$ H, $C_1 = C_2 = C_3 = 0.1\,\mu$F, and $C = 0.2\,\mu$F. For plots (a) $R_2 = 5.0\,\Omega$ and $R_3 = 2.0\,\Omega$; (b) $R_2 = 15\,\Omega$ and $R_3 = 2.0\,\Omega$; (c) $R_2 = 30\,\Omega$ and $R_3 = 5.0\,\Omega$; and (d) $R_2 = 50\,\Omega$ and $R_3 = 5.0\,\Omega$. respectively. The solid line represents P_R, whereas the dashed line represents P_X. P is given in arbitrary units.

EIT dips in the absorption line occurred when L_3 was increased, as shown in FIG. 7(b). The dispersion line also moved apart, showing the typical dispersion characteristics of double EIT. This showed how the second dip moved toward the left in comparison to the one displayed in plot 7(a). The separation of the two EIT dips is shown more clearly in FIG. 7(c) for a different set of parameters L_2 and L_3. The two dips moved in opposite directions, and double EIT was visible again. The dispersion curve also showed double EIT, and the peaks moved in opposite directions. Figure 7(d) shows the dips shifted to the right for yet another different set of parameters L_2 and L_3.

Different values of the radiative decay parameters (damping) also changed the absorption and dispersion curves in double EIT. In the electrical analogue of the atom, the resistance in the circuit loops represented the damping. A comparison of FIG. 8(a) and 8(b) shows how the first EIT dip became less pronounced, and its width expanded when resistance R_2 increased. When we increased R_2 and R_3 even more, both EIT dips became even less pronounced, and their widths increased with the resistance increase [compare FIG. 8(a) and 8(c)]. A large value of R_2 caused the first dip to spread out increasing its width and decreasing its depth.

By removing one of the loops, i.e., either $R_2L_2C_{e2}$ or $R_3L_3C_{e3}$, we recovered the two RLC coupled circuits showing single EIT (see FIG. 4). Figure 9[(a)–(d)] show the behavior of P_R and P_X after disconnecting the pumping loop $R_3L_3C_{e3}$. Plot 9(a) clearly shows a single EIT dip at exact resonance. The frequency detunings of the two RLC loops were zero; the two loops had the same resonance frequency determined from the selected parameters of each loop. By changing the value of L_2, the resonance frequencies of the two loops changed, and so did the absorption and dispersion curves, as shown in FIG. 9(b). The symmetry of the curves was lost because of the frequency detunings of the two circuits. A further increase in the L_2 value shifted the EIT dip even further [compare FIG. 9(c) with 9(b)]. In contrast, when the value of L_2 was decreased relative to L_1, the EIT dip moved in the opposite direction [FIG. 9(d)] as if there were a negative frequency detuning between the two circuit loops in comparison to plots 9(b) and 9(c).

On the other hand, the experimental results obtained for the coupled RLC circuit shown in FIG. 4(b) displayed single EIT behavior. We measured the current flowing through the resistor R_1 and calculated the power delivered to the $R_1L_1C_{e1}$ loop. Figure 8 shows the power transmitted P_R as a function of the driving field frequency ω.

In FIG. 10(a) and 10(b), the curves A and B illustrate the situation when we opened the switch SW (driven single RLC circuit), and when we closed it (driven RLC circuit coupled to a second RLC circuit). With the open switch, no power was transferred from the circuit loop $R_2L_2C_{e2}$, and the circuit loop $R_1L_1C_{e1}$ behaved like a simple, driven RLC circuit as shown in the figures. However, with the closed switch, we clearly observed a dip (curves B of these two plots). This dip resembled the single EIT-like dip shown in FIG. 9[(a)–(d)]. The two B

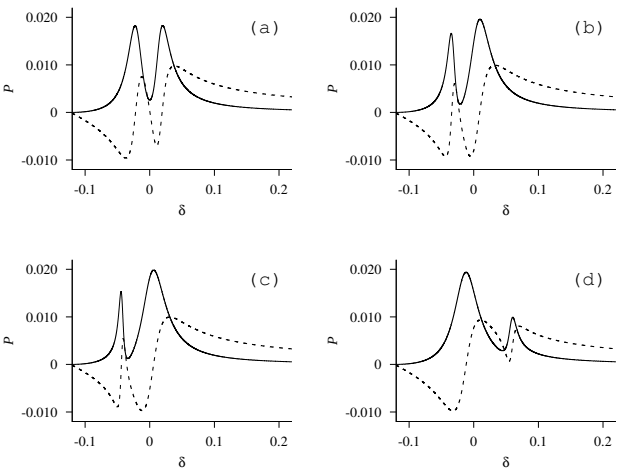

FIG. 9. Power transferred to the $R_1L_1C_{e1}$ circuit (Fig.4(b)) as a function of the detuning δ. The parameters used were $R_2 = 5.0\,\Omega$, $R_1 = 50\,\Omega$, $C_1 = C_2 = 0.1\,\mu$F, $C = 0.2\,\mu$F, and $L_1 = 0.0010$ H. For plots (a) $L_2 = 0.0010$ H, (b) $L_2 = 0.0015$ H, (c) $L_2 = 0.0020$ H, and (d) $L_2 = 0.0005$ H. The solid line represents P_R, whereas the dashed line represents P_X. P is given in arbitrary units.

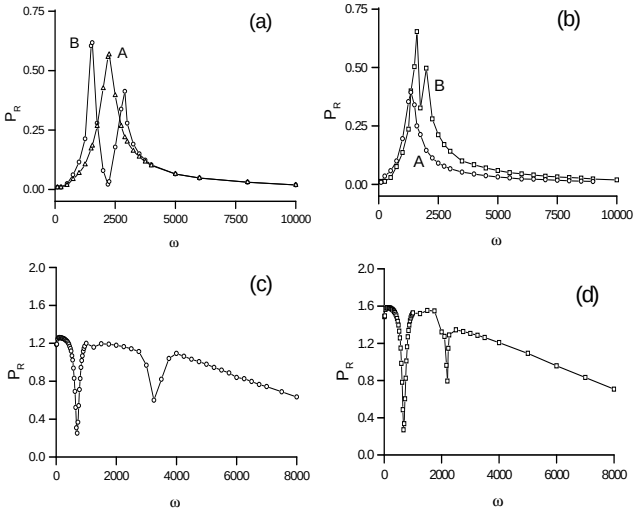

FIG. 10. Experimental plots of the power transferred P_R to the $R_1L_1C_{e1}$ loop as a function of the driving field frequency ω. Plots (a) and (b) show single EIT-like behavior, whereas (c) and (d) show double EIT. The curves A and B depict the situation when switch SW is open and closed, respectively. The parameters for this circuit are $R_1 = 50\,\Omega$, $R_2 = 5.0\,\Omega$, $C_1 = C_2 = 0.10\,\mu$F, and $L_1 = L_2 = 0.27$ H. For plots (a) $C = 0.047\,\mu$F, (b) $C = 0.2\,\mu$F. For plots (c) and (d), the parameters of the circuit are $R_1 = 87\,\Omega$, $R_2 = 16.0\,\Omega$, $R_3 = 25\,\Omega$, $C_1 = C_2 = C_3 = 0.047\,\mu$F, $C = 0.1\,\mu$F, and $L_1 = 0.27$ H. In particular, for (c) $L_2 = 0.065$ H, and (d) $L_2 = 0.185$ H, with $L_1 = L_3 = 0.27$ H

curves observed in FIG. 10 (a) and (b), essentially represented different resonance frequencies for the observed single EIT in the RLC circuits.

Note that such a simulation of single EIT along with experimental demonstrations have also been presented in an earlier work by Garrido Alzar et al.[22] They present a classical analogue of EIT using two coupled harmonic oscillators subject to a harmonic driving force [similar to FIG. 3(b)] and reproduce the phenomenology observed in EIT by changing the strength of the coherent coupling field. Moreover, these authors also recreate EIT behavior experimentally using two linearly coupled RLC circuits [similar to FIG. 4(b)]. In their work, the simulations are for the degenerate probe and coupling transitions, showing excellent agreement of the theoretical modeling of EIT (using coupled RLC circuits) with experimental results under similar conditions of parameters. In this paper, we have presented not only an extensive simulation of EIT, including the effects of different strengths of coupling fields and frequency detunings associated with the coupled harmonic oscillators and RLC circuits, but also simulations for a richer phenomenon of double EIT. We have selected different sets of parameters in the experimental simulations to show that single EIT [see FIG. 10(a,b)] and double EIT [see FIG. 10(c,d) to be discussed in the following paragraph] are exhibited for a wider range of parameters, and hence they are quite versatile.

We observed double EIT in the three coupled RLC circuits as shown in FIG. 4(a). When we experimentally measured the power transferred to the $R_1L_1C_{e1}$ loop from the loops $R_2L_2C_{e2}$ and $R_3L_3C_{e3}$, two dips were visible [see FIG. 10 (c) and (d)]. We also noted that the position of the second EIT peak changed for different values of the inductance L_2. These dips were the analogues of quantum interference observed in double EIT atomic systems. In this case, the interference happened because of the power delivered to the resonant $R_1L_1C_{e1}$ circuit from the voltage source V and the other two coupled circuits $R_2L_2C_{e2}$ and $R_3L_3C_{e3}$. Classically, we looked at this phenomena as the interference between three excitation paths corresponding to the normal modes of oscillation of the coupled harmonic oscillators.

III. SUMMARY

We have presented mechanical and electrical analogies for single, and double EIT observed in three- and four-level atomic systems using coupled harmonic oscillator models and RLC circuits. The mechanical analogy, consisting of a coupled spring-mass system, may be helpful in understanding the observed zero power absorption in single and double EIT phenomena, as a result of destructive interference between the normal modes of oscillation of the system. The dissipation rates of the coupling and pumping oscillators (γ_2 and γ_3, respectively) should be small compared with that of the atomic oscillator (γ_1) for EIT to be observable. The symmetry of the equation of

motion of the atom for EIT allows us to study easily, the absorption and dispersion of a multilevel system in the inverted-Y (four-level) and Λ (three-level) configurations.

The electrical analogy, associated with a coupled RLC circuit, may be helpful to realize the single and double EIT phenomena experimentally. This type of circuit corresponds to the electrical analogue of the mass-spring system. This fact allows us to establish a direct correspondence between an atomic system (based on the Lorentz's approximations) and the RLC circuit. In fact, by changing some circuit parameters like the inductances and capacitances, it is possible to produce different control fields acting on different atomic transitions. The resistances of the circuit represent the radiative decays of these atomic levels. The Rabi frequencies of these control fields should be large enough from the radiative decays for EIT to be observable.

The interest on these experiments, and the final purpose of this work is to help undergraduate students to develop a better understanding of single and double EIT, as well as to improve their experimental skills. These experiments are easy to adopt in any undergraduate physics laboratory, and can be used to approach other compelling topics such as quantum coherence and quantum interference, which occur in atomic systems, and are particularly important in observing phenomena like group velocity reduction of light, superconductivity and superfluidity, and quantum information processing.

ACKNOWLEDGMENTS

The authors gratefully acknowledge the Research Corporation, the College of Sciences and the Department of Physics at Eastern Illinois University, and the School of Mathematical and Natural Sciences at the University of Arkansas-Monticello for providing funding and support for this work.

* ajoshi@eiu.edu
† serna@uamont.edu

[1] S. E. Harris, "Electromagnetically induced transparency," Phys. Today **50**, 36–42 (1997); M. Fleischhauer, A. Imamoğlu, and J. P. Marangos, "Electromagnetically induced transparency: Optics in coherent media," Rev. Mod. Phys. **77**, 633–673 (2005).

[2] K. J. Boller, A. Imamoğlu, and S. E. Harris, "Observation of electromagnetically induced transparency," Phys. Rev. Lett. **66**, 2593–2596 (1991).

[3] O. Firstenberg, M. Shuker, R. Pugatch, D. R. Fredkin, N. Davidson, and A. Ron, "Theory of thermal motion in electromagnetically induced transparency: Effects of diffusion, Doppler broadening, and Dicke and Ramsey narrowing," Phys. Rev. A **77**, 043830 (2008); Y. Zhang, Z. Nie, H. Zheng, C. Li, J. Song, and M. Xiao, "Electromagnetically induced spatial nonlinear dispersion of four-wave mixing," *ibid.* **80**, 013835 (2009).

[4] A. G. Litvak and M. D. Tokman, "Electromagnetically induced transparency in ensembles of classical oscillators," Phys. Rev. Lett. **88**, 095003 (2002); G. Shvets and J. S. Wurtele, "Transparency of magnetized plasma at the cyclotron frequency," *ibid.* **89**, 115003 (2002).

[5] M. J. Werner and A. Imamoğlu, "Photon-photon interactions in cavity electromagnetically induced transparency," Phys. Rev. A **61**, 011801 (1999); C. L. Bentley, J. Liu, and Y. Liao, "Cavity electromagnetically induced transparency of driven-three-level atoms: A transparent window narrowing below a natural width," *ibid.* **61**, 023811 (2000); A. Dantan and M. Pinard, "Quantum-state transfer between fields and atoms in electromagnetically induced transparency," *ibid.* **69**, 043810 (2004); W. Yang, A. Joshi, and M. Xiao, "Chaos in an electromagnetically induced transparent medium inside an optical cavity," Phys. Rev. Lett. **95**, 093902 (2005).

[6] L. M. Kuang, Z. B. Chen, and J. W. Pan, "Generation of entangled coherent states for distant Bose-Einstein condensates via electromagnetically induced transparency," Phys. Rev. A **76**, 052324 (2007); J. O. Weatherall, C. P. Search, and M. Jääskeläinen, "Quantum control of electromagnetically induced transparency dispersion via atomic tunneling in a double-well Bose-Einstein condensate," *ibid.* **78**, 013830 (2008).

[7] K. Yamamoto, K. Ichimura, and N. Gemma, "Enhanced and reduced absorptions via quantum interference: Solid system driven by a rf field," Phys. Rev. A **58**, 2460–2466 (1998); A. Joshi, A. Brown, H. Wang, and M. Xiao, "Controlling optical bistability in a three-level atomic system," *ibid.* **67**, 041801 (2003); A. W. Brown and M. Xiao, "Modulation transfer in an electromagnetically induced transparency system," *ibid.* **70**, 053830 (2004); L. Yang, L. Zhang, X. Li, L. Han, G. Fu, N. B. Manson, D. Suter, and C. Wei, "Autler-Townes effect in a strongly driven electromagnetically induced transparency resonance," *ibid.* **72**, 053801 (2005); A. J. Olson and S. K. Mayer, "Electromagnetically induced transparency in rubidium," Am. J. Phys. **77**, 116–121 (2009).

[8] A. Joshi and M. Xiao, "Electromagnetically induced transparency and its dispersion properties in a four-level inverted-Y atomic system.." Phys. Lett. A **317**, 370 (2003); Y. Zhang, A. W. Brown, and M. Xiao, "Opening four-wave mixing and six-wave mixing channels via dual electromagnetically induced transparency windows," Phys. Rev. Lett. **99**, 123603 (2007); S. Li, X. Yang, X. Cao, C. Zhang, C. Xie, and H. Wang, "Enhanced cross-phase modulation based on a double electromagnetically induced transparency in a four-level tripod atomic system," *ibid.* **101**, 073602 (2008); A. Joshi, "Phase-dependent electromagnetically induced transparency and its dispersion properties in a four-level quantum well system," Phys. Rev. B **79**, 115315 (2009).

[9] M. Xiao, Y. Q. Li, S. Z. Jin, and J. Gea-Banacloche, "Measurement of dispersive properties of electromagnetically induced transparency in rubidium atoms," Phys. Rev. Lett. **74**, 666–669 (1995).

[10] L. V. Hau, S. E. Harris, Z. Dutton, and C. H. Behroozi,

"Light speed reduction to 17 m/s in an ultracold atomic gas," Nature **397**, 594–598 (1999).

[11] C. Liu, Z. Dutton, C. H. Behroozi, and L. V. Hau, "Observation of coherent optical information storage in an atomic medium using halted light pulses," Nature **409**, 490–493 (2001).

[12] J. Mompart and R. Corbalán, "Lasing without inversion," J. Opt. B: Quantum Semiclassical Opt. **2**, R7 (2000); H. Wu, M. Xiao, and J. Gea-Banacloche, "Evidence of lasing without inversion in a hot rubidium vapor under electromagnetically-induced-transparency conditions," Phys. Rev. A **78**, 041802 (2008).

[13] H. Wang, D. Goorskey, and M. Xiao, "Enhanced Kerr nonlinearity via atomic coherence in a three-level atomic system," Phys. Rev. Lett. **87**, 073601 (2001).

[14] H. Schmidt and R. J. Ram, "All-optical wavelength converter and switch based on electromagnetically induced transparency," Appl. Phys. Lett. **76**, 3173–3175 (2000); C. Ottaviani, D. Vitali, M. Artoni, F. Cataliotti, and P. Tombesi, "Polarization qubit phase gate in driven atomic media," Phys. Rev. Lett. **90**, 197902 (2003).

[15] G. Hétet, A. Peng, M. T. Johnsson, J. J. Hope, and P. K. Lam, "Characterization of electromagnetically-induced-transparency-based continuous-variable quantum memories," Phys. Rev. A **77**, 012323 (2008).

[16] P. Bermel, A. Rodríguez, S. G. Johnson, J. D. Joannopoulos, and M. Soljačić, "Single-photon all-optical switching using waveguide-cavity quantum electrodynamics," Phys. Rev. A **74**, 043818 (2006).

[17] D. Dragoman and M. Dragoman, *Quantum-Classical Analogies* (Springer, Berlin, 2004).

[18] P. R. Hemmer and M. G. Prentiss, "Coupled-pendulum model of the stimulated resonance Raman effect," J. Opt. Soc. Am. B **5**, 1613–1623 (1988).

[19] B. W. Shore, M. V. Gromovyy, L. P. Yatsenko, and V. I. Romanenko, "Simple mechanical analogs of rapid adiabatic passage in atomic physics," Am. J. Phys. **77**, 1183–1194 (2009).

[20] Y. Zhu, D. J. Gauthier, S. E. Morin, Q. Wu, H. J. Carmichael, and T. W. Mossberg, "Vacuum rabi splitting as a feature of linear-dispersion theory: Analysis and experimental observations," Phys. Rev. Lett. **64**, 2499–2502 (1990).

[21] J. A. Vaccaro and A. Joshi, "Position-momentum and number-phase wigner functions and their respective displacement operators," Phys. Lett. A **243**, 13–19 (1998).

[22] C. L. Garrido Alzar, M. A. G. Martínez, and P. Nussenzveig, "Classical analog of electromagnetically induced transparency," Am. J. Phys. **70**, 37–41 (2002).

[23] R. Lifshitz and M. C. Cross, "Response of parametrically driven nonlinear coupled oscillators with application to micromechanical and nanomechanical resonator arrays," Phys. Rev. B **67**, 134302 (2003).

[24] L. Allen and J. H. Eberly, *Optical Resonance and Two-Level Atoms* (Dover, New York, 1987).

[25] D. Petrosyan and G. Kurizki, "Symmetric photon-photon coupling by atoms with Zeeman-split sublevels," Phys. Rev. A **65**, 033833 (2002).

[26] S. H. Autler and C. H. Townes, "Stark effect in rapidly varying fields," Phys. Rev. **100**, 703–722 (1955).

[27] Yong-qing Li and Min Xiao, "Electromagnetically induced transparency in a three-level λ-type system in rubidium atoms," Phys. Rev. A **51**, R2703–R2706 (1995).

[28] S. Li, X. Yang, X. Cao, C. Xie, and H. Wang, "Two electromagnetically induced transparency windows and an enhanced electromagnetically induced transparency signal in a four-level tripod atomic system," J. Phys. B: At. Mol. Opt. Phys. **40**, 3211 (2007).

[29] H. A. Lorentz, *The Theory of Electrons* (Dover, New York, 1952) Chap. 4.

[30] A. P. French, *Vibrations and Waves* (Norton, New York, 1971) pp. 96–101.

[31] M. O. Scully and M. S. Zubairy, *Quantum Optics* (Cambridge University Press, Cambridge, New York, 1997) pp. 2–9.

[32] J. B. Marion and S. T. Thornton, *Classical Dynamics of Particles and Systems*, 4th ed. (Saunders, Fort Worth, Philadelphia, 1995) pp. 131–137.

[33] K. R. Symon, *Mechanics*, 3rd ed. (Addison-Wesley, Reading, Mass., 1971) p. 201.